

# Single-photon filtering by a cavity quantum electrodynamics system

Kazuki Koshino\*

College of Liberal Arts and Sciences, Tokyo Medical and Dental University, 2-8-30 Konodai, Ichikawa 272-0827, Japan  
and PRESTO, Japan Science and Technology Agency, 4-1-8 Honcho Kawaguchi, Saitama 332-0012, Japan

(Received 1 August 2007; published 5 February 2008)

The nonlinear dynamics of a classical photon pulse in a cavity-QED system is investigated theoretically. It is shown that this system can work as a single-photon filter, which drastically suppresses the multiple-photon probability of the output. The output photon statistics is sensitive to the input pulse length. A suitable choice of pulse length produces a photon pulse with the single-photon probability of 0.32, while the multiple-photon probability is suppressed to 0.01.

DOI: [10.1103/PhysRevA.77.023805](https://doi.org/10.1103/PhysRevA.77.023805)

PACS number(s): 42.50.Pq, 42.50.Gy, 42.50.Ar

## I. INTRODUCTION

Single photons are regarded as a promising candidate for qubits in quantum information processing, because photons can maintain quantum coherence for a long time. Therefore, extensive efforts have been made in generating and detecting single photons, and remarkable improvements have been reported in this field [1–7]. However, the generation of single photons on demand is still a difficult experimental task, and attenuated laser pulses (weak classical pulses) are used as a substitute for single photons in quantum key distribution [8–12]. A problem in using classical pulses is that pulses containing multiple photons may be abused by eavesdroppers [8–10]. In order to suppress the multiple-photon probability, a highly attenuated pulse must be used, in which the single-photon probability is also suppressed. For example, in order to suppress the multiple-photon probability to less than 0.01, the single-photon probability must be less than 0.14, considering Poissonian photon statistics of classical pulses. However, for efficient information processing, a pulse with a larger single-photon probability is greatly desired.

Photon statistics can be controlled by utilizing nonlinear optical effects. In particular, for the purpose of suppressing the multiple-photon probability, the photon blockade effect is promising [13–17]. In systems showing the photon blockade effect, excitation by a first photon blocks absorption of another photon while the system is excited. Therefore, it is natural to expect that when a classical pulse with a short coherence length is input, the photon blockade mechanism would filter out the multiple-photon component in the output. From this perspective, we clarify in this study how a classical pulse is transformed after transmission through a photon blockade system, based on a rigorous multimode analysis [18–21]. It is shown that using a weak classical pulse and a photon blockade system, a photon pulse can be generated having the single-photon probability of 0.32 while the multiple-photon probability is suppressed to 0.01. Namely, a photon blockade system is shown to work as a single-photon filter, which can substantially improve the efficiency of information processing.

## II. SYSTEM

### A. Hamiltonian

As the simplest photon blockade system, we consider in this study a two-level atom placed inside a two-sided cavity, as illustrated in Fig. 1. Setting  $\hbar=c=1$ , taking the atomic resonance as the origin of the energy, and taking the dissipationless limit ( $\gamma \rightarrow 0$ ) for simplicity, the Hamiltonian of the whole system including the external photon field is given by

$$\mathcal{H} = g(\sigma^\dagger c + c^\dagger \sigma) + \int dk [k a_k^\dagger a_k + \sqrt{\kappa/2\pi}(c^\dagger a_k + a_k^\dagger c)] + \int dk [k b_k^\dagger b_k + \sqrt{\kappa/2\pi}(c^\dagger b_k + b_k^\dagger c)], \quad (1)$$

where  $g$  and  $\kappa$  represent the vacuum Rabi frequency and the cavity decay rate, respectively. (The escape rates of a cavity photon into the left- and right-hand sides are identical.)  $\sigma$  and  $c$  denote the annihilation operators for the atomic excitation and the cavity photon, respectively, and  $a_k$  and  $b_k$  denote the annihilation operators for the external photon mode with energy  $k$ , extending in the left- and right-hand sides of the cavity, respectively.  $c$ ,  $a_k$ , and  $b_k$  are the bosonic operators satisfying  $[c, c^\dagger]=1$  and  $[a_k, a_{k'}^\dagger]=[b_k, b_{k'}^\dagger]=\delta(k-k')$ , whereas  $\sigma$  is the Pauli operator satisfying  $[\sigma, \sigma^\dagger]=1-2\sigma^\dagger\sigma$ . The real-space representation of  $a_k$ , denoted hereafter by  $\tilde{a}_r$ , is given by

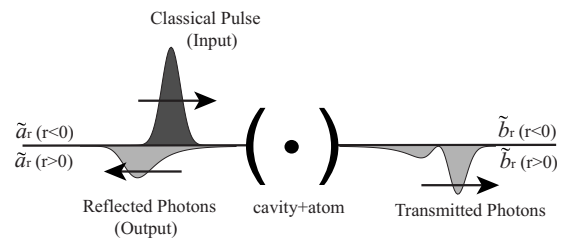


FIG. 1. Schematic illustration of the situation considered in this study. A classical pulse is input from the left-hand side of a two-sided cavity containing a two-level atom. Photons emitted in the reflection direction are regarded as the output.

\*ikuzak.las@tmd.ac.jp

$$\tilde{a}_r = (2\pi)^{-1/2} \int dk e^{ikr} a_k. \quad (2)$$

$\tilde{b}_r$  is defined similarly. As illustrated in Fig. 1, the  $r < 0$  and  $r > 0$  regions correspond to the incoming and outgoing fields, respectively.

Throughout this study, we consider the weak-coupling case, characterized by  $\kappa \gg g$  [22]. As will be shown in the Appendix, the dynamics in this case is characterized solely by the atomic decay rate  $\Gamma$ , which is given by

$$\Gamma = g^2/\kappa. \quad (3)$$

### B. State vector of input photons

In this study, we investigate the following situation: A classical light pulse is input from the left-hand side of the cavity (the  $r < 0$  region of  $\tilde{a}_r$ ), whereas no light pulse is input from the right-hand side (the  $r < 0$  region of  $\tilde{b}_r$ ), and photons emitted in the reflection direction (the  $r > 0$  region of  $\tilde{a}_r$ ) are regarded as the output. The amplitude of the input pulse (at the initial moment,  $\tau=0$ ) is denoted by  $\alpha f(r)$ , where the input mode function  $f(r)$  is normalized as  $\int dr |f(r)|^2 = 1$  and is localized in the  $r < 0$  region, and  $|\alpha|^2$  represents the mean photon number. The state vector of the input pulse is given by

$$|\Phi_{\text{in}}\rangle = \mathcal{N} \exp\left(\alpha \int dr f(r) \tilde{a}_r^\dagger\right) |0\rangle, \quad (4)$$

where  $\mathcal{N}$  is the normalization constant, given by  $\mathcal{N} = \exp(-|\alpha|^2/2)$ . The input state vector can be expanded as

$$|\Phi_{\text{in}}\rangle = \mathcal{N}(|0\rangle + \alpha|1_{\text{in}}\rangle + 2^{-1/2}\alpha^2|2_{\text{in}}\rangle + \dots), \quad (5)$$

where  $|n_{\text{in}}\rangle$  is the  $n$ -photon Fock state for the mode function  $f(r)$ , given by  $|n_{\text{in}}\rangle = (n!)^{-1/2} [\int dr f(r) \tilde{a}_r^\dagger]^n |0\rangle$ .

### C. State vector of output photons

The output state vector (at the final moment  $\tau=t$ , where  $t$  is a sufficiently long time) is given by  $|\Phi_{\text{out}}\rangle = e^{-iHt} |\Phi_{\text{in}}\rangle$ . From the linearity of the quantum time evolution and the photon number conservation in the present system, the output state vector takes the same form as Eq. (5),

$$|\Phi_{\text{out}}\rangle = \mathcal{N}(|0\rangle + \alpha|1_{\text{out}}\rangle + 2^{-1/2}\alpha^2|2_{\text{out}}\rangle + \dots). \quad (6)$$

In the output state, both transmitted and reflected photons exist. Therefore,  $|n_{\text{out}}\rangle$  can be written as

$$|n_{\text{out}}\rangle = \sum_{j=0}^n \int d^n r \frac{\tilde{g}_{n;j}(r_1, \dots, r_n)}{\sqrt{j!(n-j)!}} \langle \tilde{a}_{r_1}^\dagger \dots \tilde{a}_{r_j}^\dagger \tilde{b}_{r_{j+1}}^\dagger \dots \tilde{b}_{r_n}^\dagger |0\rangle, \quad (7)$$

where  $\tilde{g}_{n;j}(r_1, \dots, r_n)$  is the  $n$ -photon output wave function with  $j$  reflected and  $n-j$  transmitted photons. Although the time coordinate is not explicitly shown,  $\tilde{g}$  denotes the wave function at the final moment. The probability of  $j$ -photon reflection for the  $n$ -photon input, hereafter denoted by  $p_{n;j}$ , is given by

$$p_{n;j} = \int d^n r |\tilde{g}_{n;j}(r_1, \dots, r_n)|^2, \quad (8)$$

namely, the norm of  $\tilde{g}_{n;j}$ . The probability conservation law,  $\sum_{j=0}^n p_{n;j} = 1$ , holds since  $\langle n_{\text{out}} | n_{\text{out}} \rangle = 1$ .

## III. WAVE FUNCTION OF OUTPUT PHOTONS

### A. Rules for construction of output wave functions

The  $n$ -photon output wave function  $\tilde{g}_{n;j}$  can be obtained through the correlation function in the output field [21]. In the Appendix, the detailed calculation of  $\tilde{g}_{2;1}$  is presented for example. The results can be summarized by the following three rules: (i)  $\tilde{g}_{n;j}(r_1, \dots, r_n) = \sqrt{n} C_j \langle \tilde{a}_{r_1} \dots \tilde{a}_{r_j} \tilde{b}_{r_{j+1}} \dots \tilde{b}_{r_n} \rangle$ , where  $\langle \tilde{a}_{r_1} \dots \tilde{a}_{r_j} \tilde{b}_{r_{j+1}} \dots \tilde{b}_{r_n} \rangle$  is the lowest-order component of the  $n$ -point correlation function in the output field. (ii) When calculating the correlation function,  $\tilde{b}_r$  can be replaced with  $\tilde{a}_{r-t} f(r-t)$ , where  $f(r)$  is the input mode function. Note that  $f(r)$  is a  $c$  number, whereas  $\tilde{a}_r$  is an operator. (iii)  $\langle \tilde{a}_{r_1} \dots \tilde{a}_{r_n} \rangle$  is a symmetric function of  $r_1, \dots, r_n$  by definition, and is given, for  $r_1 \leq \dots \leq r_n$ , by  $\tilde{f}(r_n) \prod_{j=1}^{n-1} [\tilde{f}(r_j) - e^{\Gamma(r_j - r_{j+1})} \tilde{f}(r_{j+1})]$ , where  $\tilde{f}(r) [= \tilde{g}_{1;1}(r)]$  is the wave function of the reflected photon for the single-photon input, given by

$$\tilde{f}(r) = \Gamma \int_0^\infty d\xi f(r-t+\xi) e^{-\Gamma\xi}. \quad (9)$$

### B. Concrete forms of output wave functions

By following these rules, the  $n$ -photon output wave function  $\tilde{g}_{n;j}$  can be expressed in terms of  $f(r)$  and  $\tilde{f}(r)$ . Here we present concrete forms of the output wave functions, up to the two-photon component. When the one-photon Fock state  $|1_{\text{in}}\rangle$  is input, the wave functions of the transmitted and reflected photons are given by

$$\tilde{g}_{1;0}(r) = \tilde{f}(r) - f(r-t), \quad (10)$$

$$\tilde{g}_{1;1}(r) = \tilde{f}(r). \quad (11)$$

When the two-photon Fock state  $|2_{\text{in}}\rangle$  is input, the output wave functions are given by

$$\tilde{g}_{2;0}(r_1, r_2) = \tilde{g}_{1;0}(r_1) \tilde{g}_{1;0}(r_2) - e^{-\Gamma|r_1 - r_2|} \tilde{f}^2(R), \quad (12)$$

$$\frac{\tilde{g}_{2;1}(r_1, r_2)}{\sqrt{2}} = \tilde{g}_{1;1}(r_1) \tilde{g}_{1;0}(r_2) - e^{-\Gamma|r_1 - r_2|} \tilde{f}^2(R), \quad (13)$$

$$\tilde{g}_{2;2}(r_1, r_2) = \tilde{g}_{1;1}(r_1) \tilde{g}_{1;1}(r_2) - e^{-\Gamma|r_1 - r_2|} \tilde{f}^2(R), \quad (14)$$

where  $R = \max(r_1, r_2)$ . The first and second terms on the right-hand side of each equation represent the linear and non-linear components, respectively.

These wave functions contain the full information of output photons. The reflection and transmission probabilities  $p_{n;j}$  can be calculated by Eq. (8). The photon statistics of the

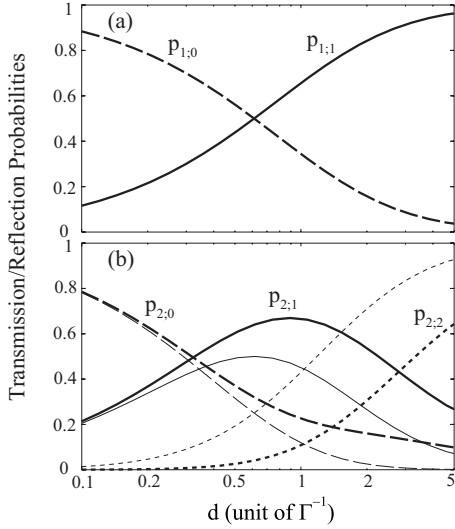


FIG. 2. Plots of the transmission and/or reflection probabilities as functions of the pulse length  $d$ ; (a) one-photon input, (b) two-photon input.  $p_{n,j}$  represents the probability of  $j$ -photon reflection for  $n$ -photon input. In (b), the transmission and/or reflection probabilities of the linear case are also plotted by thin lines for reference.

output pulse can be calculated by Eqs. (8) and (17). The intensity distribution of the output pulse can be calculated by Eq. (20).

#### IV. NUMERICAL RESULTS

##### A. Input mode function

To be more specific, we hereafter assume that the input light is in resonance with the atom and has a Gaussian mode function with pulse length  $d$ . Denoting the initial position of the pulse by  $a$  ( $a < 0$  and  $|a| \gg d$ ), the input mode function is given by

$$f(r) = \left( \frac{2}{\pi d^2} \right)^{1/4} \exp \left[ - \left( \frac{r-a}{d} \right)^2 \right]. \quad (15)$$

Then, from Eq. (9), we obtain

$$\begin{aligned} \tilde{f}(r) &= \left( \frac{\pi d^2 \Gamma^4}{8} \right)^{1/4} \exp \left( \Gamma(r-a-t) + \frac{\Gamma^2 d^2}{4} \right) \\ &\times \operatorname{erfc} \left( \frac{r-a-t}{d} + \frac{\Gamma d}{2} \right), \end{aligned} \quad (16)$$

where the complementary error function is defined by  $\operatorname{erfc}(x) = 2\pi^{-1/2} \int_x^\infty d\xi \exp(-\xi^2)$ .

##### B. Transmission and reflection probabilities

The norms of  $\tilde{g}_{1,0}$  and  $\tilde{g}_{1,1}$  give the transmission and reflection probabilities,  $p_{1,0}$  and  $p_{1,1}$ . In Fig. 2(a),  $p_{1,0}$  and  $p_{1,1}$  are plotted as functions of the pulse length  $d$ . It is observed that the reflection probability  $p_{1,1}$  increases monotonically as  $d$  is increased, and approaches unity in the limit of  $d \rightarrow \infty$ .

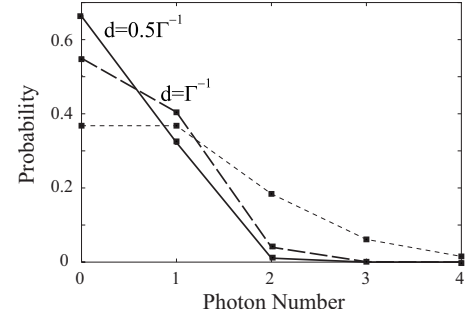


FIG. 3. Input and output photon statistics. The thin dotted line plots the input photon statistics for  $|\alpha|^2=1$ . (The input photon statistics is independent of  $d$ .) The solid and dashed lines show the output photon statistics for  $d=0.5\Gamma^{-1}$  and  $\Gamma^{-1}$ , respectively.

Thus, for efficient reflection of the single-photon component, a long pulse is advantageous.

The norms of  $\tilde{g}_{2,0}$ ,  $\tilde{g}_{2,1}$ , and  $\tilde{g}_{2,2}$  give the probabilities  $p_{2,0}$ ,  $p_{2,1}$ , and  $p_{2,2}$ , which are shown in Fig. 2(b); for reference, the correspondent probabilities of the linear case, given by  $p_{n,j}^L = {}_n C_j (p_{1,0})^{n-j} (p_{1,1})^j$ , are also plotted by thin lines.  $p_{n,j}$  agrees well with  $p_{n,j}^L$  in the small  $d$  region, in which most photons cannot be absorbed by the atom and therefore the saturation nonlinearity is weak. However, for larger  $d$ ,  $p_{n,j}$  deviates from  $p_{n,j}^L$  due to the increasing nonlinear effect. It is observed that, in comparison with the linear case, the two-photon reflection probability  $p_{2,2}$  is suppressed, while the zero- and one-photon reflection probabilities  $p_{2,0}$  and  $p_{2,1}$  increase, demonstrating the photon blockade effect.  $p_{2,2}$  increases monotonically as  $d$  is increased for two reasons: (1) the increase of the linear reflectivity  $p_{1,1}$  and (2) weakness of the blockade effect when the pulse length is large [23]. Thus, for exclusion of the two-photon component in the output, a short pulse is advantageous.

##### C. Photon statistics

The photon statistics of the output pulse is readily obtained from  $p_{n,j}$ . Here, the photon statistics is observed as a function of the pulse length  $d$  and the input intensity  $|\alpha|^2$ . Since the  $n$ -photon probability of the input pulse  $|\Phi_{\text{in}}\rangle$  is given by  $|\alpha|^{2n} e^{-|\alpha|^2} / n!$ , the  $j$ -photon probability in the output pulse is given by

$$P_j(d, \alpha) = \sum_{n=j}^{\infty} p_{n,j}(d) \frac{|\alpha|^{2n} e^{-|\alpha|^2}}{n!}. \quad (17)$$

The photon statistics of the input and output pulses are plotted in Fig. 3, where the input intensity  $|\alpha|^2$  is fixed at unity and the pulse length  $d$  is chosen to be  $0.5\Gamma^{-1}$  and  $\Gamma^{-1}$ . In the input pulse (thin dotted line in Fig. 3), the multiple-photon probability  $P_m (=P_2+P_3+\dots)$  is comparable with the single-photon probability  $P_1$  ( $P_m=0.26$ ,  $P_1=0.37$ ). In contrast, in the output pulse, the multiple-photon probability  $P_m$  is drastically suppressed, while the single-photon probability  $P_1$  is almost unchanged. For example, when  $d=0.5\Gamma^{-1}$  (solid line in Fig. 3),  $P_m=0.01$  and  $P_1=0.32$ . As expected from Fig. 2, the single-photon probability can be increased by using a

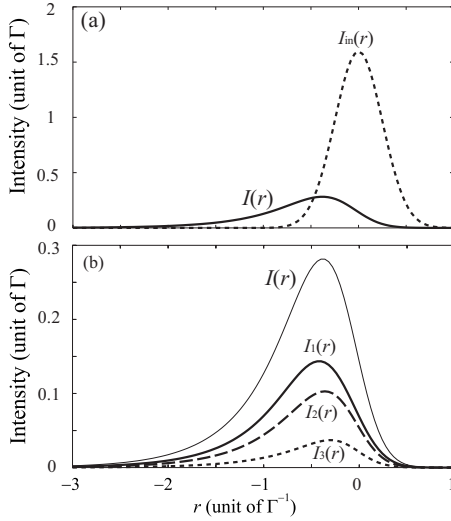


FIG. 4. (a) Intensity distributions of the input pulse (dotted line) and the output pulse (solid line), observed from a coordinate system moving at light velocity. The input pulse is characterized by  $\alpha=1$  and  $d=0.5\Gamma^{-1}$ . (b) Plots of  $I_1(r)$  (solid line),  $I_2(r)$  (dashed line), and  $I_3(r)$  (dotted line).  $I(r)$  is plotted by a thin line for reference.

longer pulse, accompanied by an increase in the multiple-photon probability. For example, when  $d=\Gamma^{-1}$  (dashed line in Fig. 3),  $P_m=0.04$  and  $P_1=0.40$ .

#### D. Intensity distribution

Since analytic forms of the output wave functions are available, we can observe the spatial shape of the photon pulse thus generated. For this purpose, we use the intensity distribution  $I(r)$  of the output pulse, given by  $I(r) = \langle \Phi_{\text{out}} | \tilde{a}_r^\dagger \tilde{a}_r | \Phi_{\text{out}} \rangle$ . Since the multiphoton probability is negligibly small,  $I(r)$  can be regarded as the intensity distribution of a single photon. Using Eq. (6), we have

$$I(r) = I_1(r) + I_2(r) + \dots, \quad (18)$$

$$I_n(r) = \frac{e^{-|\alpha|^2} |\alpha|^{2n}}{n!} \langle n_{\text{out}} | \tilde{a}_r^\dagger \tilde{a}_r | n_{\text{out}} \rangle. \quad (19)$$

Namely,  $I_n(r)$  describes the intensity distribution of a single photon that originates from  $|n_{\text{in}}\rangle$ . In terms of the output wave function  $\tilde{g}_{n,j}$ , after tracing out the variables  $r'$  for the transmitted photons,  $I_n(r)$  is given by

$$I_n(r) = \frac{e^{-|\alpha|^2} |\alpha|^{2n}}{n!} \int d^{n-1} r' |\tilde{g}_{n,1}(r, r'_1, \dots, r'_{n-1})|^2. \quad (20)$$

In Fig. 4(a), the intensity distribution  $I(r)$  of the output pulse is compared with that of the input, given by  $I_{\text{in}}(r) = \langle \Phi_{\text{in}} | \tilde{a}_r^\dagger \tilde{a}_r | \Phi_{\text{in}} \rangle = |\alpha|^2 |f(r)|^2$ , for  $\alpha=1$  and  $d=0.5\Gamma^{-1}$ . It is observed that the output becomes much weaker than the input [ $\int dr I_{\text{in}}(r)=1$  whereas  $\int dr I(r)=0.32$ ], since a considerable fraction of the input is filtered out by this optical system. It is also observed that the output pulse is delayed in comparison with the input, due to the absorption and emission by the

atom, which takes a time of the order of  $\Gamma^{-1}$ . In Fig. 4(b),  $I_n(r)$  is plotted for  $n=1, 2$ , and 3. By evaluating  $\int dr I_n(r) / \int dr I(r)$ , it is confirmed that a generated single photon originates from  $|1_{\text{in}}\rangle$  by 51%,  $|2_{\text{in}}\rangle$  by 35%, and  $|3_{\text{in}}\rangle$  by 12%. After normalization, it is also confirmed that  $I_1(r)$ ,  $I_2(r)$ , and  $I_3(r)$  have similar spatial shapes. The delay of  $I_1(r)$  is slightly larger than those of  $I_2(r)$  and  $I_3(r)$ , since the delay mechanism (absorption and emission by the atom) per photon decreases when multiple photons are involved in the dynamics.

## V. SUMMARY

In summary, we have investigated the nonlinear dynamics of a classical photon pulse in a photon blockade system. As a photon blockade system, a two-sided cavity containing a two-level atom is considered; the photons emitted in the reflection direction are regarded as the output (Fig. 1). The wave functions of the transmitted and reflected photons are obtained analytically. Using these output wave functions, the transmission and/or reflection probabilities (Fig. 2), output photon statistics (Fig. 3), and spatial shape of the output pulse (Fig. 4) are observed. It is demonstrated that a cavity-QED system can function as a single-photon filter. When the mean photon number is unity, the single-photon probability  $P_1$  and the multiple-photon probability  $P_m$  are comparable in the input ( $P_1=0.37$  and  $P_m=0.26$ ). After transmission through the filter, the multiple-photon probability is drastically suppressed whereas the multiple-photon probability is nearly unchanged (when the pulse length  $d=0.5\Gamma^{-1}$ ,  $P_1=0.32$ , and  $P_m=0.01$ ). Such a single-photon filter would be useful for secure and efficient information processing.

## ACKNOWLEDGMENTS

The author is grateful to K. Edamatsu and S. Kono for fruitful discussions. This research was supported by the Research Foundation for Opto-Science and Technology, and by a Grant-in-Aid for Creative Scientific Research (Grant No. 17GS1204).

## APPENDIX: CALCULATION OF OUTPUT WAVE FUNCTION

### 1. Heisenberg equations

From the Hamiltonian of Eq. (1), the Heisenberg equation for  $a_k$  is given by

$$\frac{d}{d\tau} a_k = -ika_k - i\sqrt{\kappa/2\pi}c. \quad (A1)$$

Denoting the initial and final moments by 0 and  $t$ , the operator at time  $\tau$  ( $0 < \tau < t$ ) is represented in two ways,

$$a_k(\tau) = a_k(0)e^{-ik\tau} - i\sqrt{\kappa/2\pi}c \int_0^\tau d\tau' c(\tau') e^{-ik(\tau-\tau')}, \quad (A2)$$

$$a_k(\tau) = a_k(t)e^{-ik(\tau-t)} + i\sqrt{\kappa/2\pi} \int_{\tau}^t d\tau' c(\tau')e^{-ik(\tau-\tau')}. \quad (\text{A3})$$

Using Eq. (2) and the above two forms of  $a_k(\tau)$ ,  $\tilde{a}_0(\tau)$  is recast into the following two forms:

$$\tilde{a}_0(\tau) = \tilde{a}_{-\tau}(0) - i\sqrt{\kappa/2}c(\tau), \quad (\text{A4})$$

$$\tilde{a}_0(\tau) = \tilde{a}_{t-\tau}(t) + i\sqrt{\kappa/2}c(\tau). \quad (\text{A5})$$

Equating the right-hand sides and introducing a new label  $r(=t-\tau)$ , we obtain the input-output relation, as given by

$$\tilde{a}_r(t) = \tilde{a}_{r-t}(0) - i\sqrt{\kappa}c(t-r), \quad (\text{A6})$$

where  $0 < r < t$ . Thus, the output field operator at time  $t$  is expressed in terms of the input field operator at the initial moment and the cavity-mode operator at  $t-r$ . Similarly, the input-output relation for  $\tilde{b}_r$  is given by

$$\tilde{b}_r(t) = \tilde{b}_{r-t}(0) - i\sqrt{\kappa}c(t-r). \quad (\text{A7})$$

The Heisenberg equations for the atomic operator  $\sigma$  and the cavity-mode operator  $c$  are derived from the Hamiltonian of Eq. (1). Using Eq. (A4) and its counterpart for  $\tilde{b}_0(\tau)$ , they are recast into the following forms:

$$\frac{d}{d\tau}\sigma = -ig(1 - 2\sigma^\dagger\sigma)c, \quad (\text{A8})$$

$$\frac{d}{d\tau}c = -\kappa c - ig\sigma - i\sqrt{\kappa}[\tilde{a}_{-\tau}(0) + \tilde{b}_{-\tau}(0)]. \quad (\text{A9})$$

Throughout this study, a weak coupling case ( $\kappa \gg g$ ) is considered. In this case, Eq. (A9) can be solved adiabatically. The cavity operator is given by

$$c = -i(g/\kappa)\sigma - i\kappa^{-1/2}[\tilde{a}_{-\tau}(0) + \tilde{b}_{-\tau}(0)]. \quad (\text{A10})$$

Substituting Eq. (A10) into Eqs. (A6)–(A8), we obtain the following equations:

$$\tilde{a}_r(t) = -\tilde{b}_{r-t}(0) - \sqrt{\Gamma}\sigma(t-r), \quad (\text{A11})$$

$$\tilde{b}_r(t) = -\tilde{a}_{r-t}(0) - \sqrt{\Gamma}\sigma(t-r), \quad (\text{A12})$$

$$\frac{d}{d\tau}\sigma = -\Gamma\sigma - \sqrt{\Gamma}(1 - 2\sigma^\dagger\sigma)[\tilde{a}_{-\tau}(0) + \tilde{b}_{-\tau}(0)], \quad (\text{A13})$$

where  $\Gamma$  is the atomic decay rate, defined by Eq. (3). These are the basic equations for calculation of the correlation function in the output field.

## 2. Relation between the output wave function and the correlation function

Here, we investigate the relation between the output wave function and the  $n$ -point correlation function. The  $n$ -point correlation function is defined by

$\langle \Phi_{\text{out}} | \tilde{a}_{r_1} \cdots \tilde{a}_{r_j} \tilde{b}_{r_{j+1}} \cdots \tilde{b}_{r_n} | \Phi_{\text{out}} \rangle$ . We denote the lowest-order component of this correlation function, which is proportional to  $\alpha^n$ , by  $\langle \tilde{a}_{r_1} \cdots \tilde{a}_{r_j} \tilde{b}_{r_{j+1}} \cdots \tilde{b}_{r_n} \rangle$ . From Eqs. (6) and (7), the following equations can be confirmed:

$$\langle \tilde{a}_{r_1} \cdots \tilde{a}_{r_j} \tilde{b}_{r_{j+1}} \cdots \tilde{b}_{r_n} \rangle = \frac{\langle 0 | \tilde{a}_{r_1} \cdots \tilde{a}_{r_j} \tilde{b}_{r_{j+1}} \cdots \tilde{b}_{r_n} | n_{\text{out}} \rangle}{\sqrt{n!}}, \quad (\text{A14})$$

$$\tilde{g}_{n;j}(r_1, \dots, r_n) = \frac{\langle 0 | \tilde{a}_{r_1} \cdots \tilde{a}_{r_j} \tilde{b}_{r_{j+1}} \cdots \tilde{b}_{r_n} | n_{\text{out}} \rangle}{\sqrt{j!(n-j)!}}. \quad (\text{A15})$$

Combining Eqs. (A14) and (A15), we obtain

$$\tilde{g}_{n;j}(r_1, \dots, r_n) = \sqrt{n} C_j \langle \tilde{a}_{r_1} \cdots \tilde{a}_{r_j} \tilde{b}_{r_{j+1}} \cdots \tilde{b}_{r_n} \rangle. \quad (\text{A16})$$

This is the first rule presented in Sec. III A.

## 3. Calculation of the correlation function

Next, we proceed to calculate the correlation function in the lowest order. For example, we consider the two-point correlation function  $\langle \tilde{a}_{r_1} \tilde{b}_{r_2} \rangle$ . In order to calculate the correlation function, it is convenient to work in the Heisenberg representation. Namely, we use the output field operators given by Eqs. (A11) and (A12), and the initial state vector given by Eq. (4). Then,  $\langle \tilde{a}_{r_1} \tilde{b}_{r_2} \rangle$  is recast into the following form:

$$\langle \tilde{a}_{r_1} \tilde{b}_{r_2} \rangle = \alpha \sqrt{\Gamma} f(r_2 - t) \langle \sigma(t - r_1) \rangle + \Gamma \langle \sigma(t - r) \sigma(t - R) \rangle, \quad (\text{A17})$$

where  $r = \min(r_1, r_2)$  and  $R = \max(r_1, r_2)$ . The following two facts should be remarked in derivation of the above equation: (i) the input-field operators  $\tilde{a}_r(0)$  and  $\tilde{b}_r(0)$  commute with  $\sigma(t)$  if  $r+t < 0$ , and (ii) the input-field operators can be replaced with  $c$  numbers [ $\tilde{a}_r(0) \rightarrow \alpha f(r)$  and  $\tilde{b}_r(0) \rightarrow 0$ ] since the input state vector  $|\Phi_{\text{in}}\rangle$  is an eigenstate of the input-field operators. Equation (A17) demonstrates that the field correlation function  $\langle \tilde{a}_{r_1} \tilde{b}_{r_2} \rangle$  is composed of the input mode function,  $f(r)$ , and the atomic correlation functions,  $\langle \sigma(\tau) \rangle$  and  $\langle \sigma(\tau) \sigma(\tau') \rangle$ .

The atomic correlation function can be calculated by using Eqs. (4) and (A13). The equation of motion for  $\langle \sigma(t) \rangle$  is given by

$$\frac{d}{d\tau} \langle \sigma \rangle = -\Gamma \langle \sigma \rangle - \alpha \sqrt{\Gamma} f(-\tau). \quad (\text{A18})$$

Note that the third-order term has been removed in the above equation, since we are concerned with only the linear component. By integrating Eq. (A18), we obtain

$$\langle \sigma(\tau) \rangle = -\frac{\alpha}{\sqrt{\Gamma}} \tilde{f}(t - \tau), \quad (\text{A19})$$

where  $\tilde{f}$  is defined in Eq. (9).

From Eqs. (4) and (A13), the equation of motion for  $\langle\sigma(\tau)\sigma(\tau')\rangle$  for  $\tau > \tau'$  is given by

$$\frac{d}{d\tau}\langle\sigma(\tau)\sigma(\tau')\rangle = -\Gamma\langle\sigma(\tau)\sigma(\tau')\rangle - \alpha\sqrt{\Gamma}f(-\tau)\langle\sigma(\tau')\rangle. \quad (\text{A20})$$

Note that the fourth-order term has been removed. The solution of Eq. (A20), satisfying the initial condition of  $\langle\sigma(\tau')\sigma(\tau')\rangle=0$ , is given by

$$\langle\sigma(\tau)\sigma(\tau')\rangle = \langle\sigma(\tau)\rangle\langle\sigma(\tau')\rangle - \langle\sigma(\tau')\rangle^2 e^{-\Gamma(\tau-\tau')}. \quad (\text{A21})$$

Combining Eqs. (A16), (A17), (A19), and (A21), and removing the perturbation coefficient  $\alpha^2$ , we finally obtain

$$\frac{\tilde{g}_{2;1}(r_1, r_2)}{\sqrt{2}} = \tilde{f}(r_1)[\tilde{f}(r_2) - f(r_2 - t)] - e^{-\Gamma|r_1 - r_2|}\tilde{f}^2(R). \quad (\text{A22})$$

Thus, Eq. (13) is reproduced. Extension to general  $\tilde{g}_{n,j}$  is straightforward. The results can be summarized by the three rules presented in Sec. III A.

- 
- [1] O. Benson, C. Santori, M. Pelton, and Y. Yamamoto, Phys. Rev. Lett. **84**, 2513 (2000).
- [2] Z. Yuan, B. E. Kardynal, R. M. Stevenson, A. J. Shields, C. J. Lobo, K. Cooper, N. S. Beattie, D. A. Ritchie, and M. Pepper, Science **295**, 102 (2002).
- [3] M. Keller, B. Lange, K. Hayasaka, W. Lange, and H. Walther, Nature (London) **431**, 1075 (2004).
- [4] J. McKeever, A. Boca, A. D. Boozer, R. Miller, J. R. Buck, A. Kuzmich, and H. J. Kimble, Science **303**, 1992 (2004).
- [5] N. Namekata, Y. Makino, and S. Inoue, Opt. Lett. **27**, 954 (2002).
- [6] A. Tomita and K. Nakamura, Opt. Lett. **27**, 1827 (2002).
- [7] C. Langrock, E. Diamanti, R. V. Roussev, Y. Yamamoto, M. M. Fejer, and H. Takesue, Opt. Lett. **30**, 1725 (2005).
- [8] B. Huttner, N. Imoto, N. Gisin, and T. Mor, Phys. Rev. A **51**, 1863 (1995).
- [9] G. Brassard, N. Lutkenhaus, T. Mor, and B. C. Sanders, Phys. Rev. Lett. **85**, 1330 (2000).
- [10] N. Lutkenhaus, Phys. Rev. A **61**, 052304 (2000).
- [11] W.-Y. Hwang, Phys. Rev. Lett. **91**, 057901 (2003).
- [12] X.-B. Wang, Phys. Rev. Lett. **94**, 230503 (2005).
- [13] A. Imamoglu, H. Schmidt, G. Woods, and M. Deutsch, Phys. Rev. Lett. **79**, 1467 (1997).
- [14] P. Grangier, D. F. Walls, and K. M. Gheri, Phys. Rev. Lett. **81**, 2833 (1998).
- [15] M. J. Werner and A. Imamoglu, Phys. Rev. A **61**, 011801(R) (1999).
- [16] S. Rebic, A. S. Parkins, and S. M. Tan, Phys. Rev. A **65**, 063804 (2002).
- [17] K. M. Birnbaum, A. Boca, R. Miller, A. D. Boozer, T. E. Northup, and H. J. Kimble, Nature (London) **436**, 87 (2005).
- [18] K. Koshino and H. Ishihara, Phys. Rev. Lett. **93**, 173601 (2004).
- [19] J. H. Shapiro and R. S. Bondurant, Phys. Rev. A **73**, 022301 (2006).
- [20] J. H. Shapiro, Phys. Rev. A **73**, 062305 (2006).
- [21] K. Koshino, Phys. Rev. Lett. **98**, 223902 (2007).
- [22] Q. A. Turchette, C. J. Hood, W. Lange, H. Mabuchi, and H. J. Kimble, Phys. Rev. Lett. **75**, 4710 (1995).
- [23] When a resonant continuous wave is input, the normalized second-order correlation function  $g^{(2)}(\tau)$  of the output is given by  $g^{(2)}(\tau) = (1 - e^{-\Gamma\tau})^2$  in this system. Therefore, the photon blockade mechanism becomes weaker when  $d \geq \Gamma^{-1}$ .